This manuscript has been published in EARTH AND PLANETARY SCIENCE LETTERS.

https://doi.org/10.1016/j.epsl.2025.119489

Assessing the timing of deep ocean oxygenation from uranium elemental and isotopic compositions of ophiolites

Joel B. Rodney[a*], Morten B. Andersen[b], Daniel Stubbs[a, c], C. Johan Lissenberg[b], Omar Gianola[d], Matthias Willbold[e], Tim Elliott[a]

[a]Bristol Isotope Group, School of Earth Sciences, University of Bristol, Wills Memorial Building, Queen's Road, Bristol, BS8 1RJ, UK

[b]School of Earth & Environmental Sciences, Cardiff University, Park Place, Cardiff, CF10 3AT, UK

[c]National Nuclear Laboratory, Central Laboratory, Sellafield, Cumbria, UK, CA20 1PG

[d]Department of Geosciences, University of Padova, Via G. Gradenigo 6, 35131 Padova, Italy

[e]Georg-August-Universität Göttingen, Geowissenschaftliches Zentrum Göttingen, Abt. Geochemie und Isotopengeologie, Goldschmidtstr. 1, 37077 Göttingen, Germany

*Corresponding author

Email addresses: joel.rodney@bristol.ac.uk (J.B. Rodney), andersenm1@cardiff.ac.uk (M.B. Andersen), dstubbs95@icloud.com (D. Stubbs), lissenbergcj@cardiff.ac.uk (C. J. Lissenberg), omar.gianola.res@gmail.com (O. Gianola), matthias.willbold@uni-goettingen.de (M. Willbold), tim.elliott@bristol.ac.uk (T. Elliott).

Abstract

The concentration of dissolved oxygen in the deep oceans has varied over Earth History, but the timing of the transition from anoxic to oxic deep oceans is debated. Under modern-day, oxic, deep ocean conditions, alteration of the upper sections of mafic oceanic crust with U-rich seawater leads to U enrichment, low Th/U ratios, and heterogeneous $^{238}U/^{235}U$ ratios relative to fresh mid-ocean ridge basalt (MORB). Given the solubility behaviour of U, its uptake into altered oceanic crust (AOC) is expected to be smaller and less isotopically fractionated when deep oceans were anoxic and thus U-poor. Determining when, in the geological record, the U elemental and isotopic systematics of ancient oceanic crust first resemble modern day AOC should indicate when deep oceans became oxic. We provide U concentration, Th/U, and U isotopic data on upper-crustal sections of three ophiolites from 750 to 480 Ma, spanning the period inferred for deep ocean oxygenation (~ 850 to 400 Ma). The ophiolites at 480 and 540 Ma have high U contents, low Th/U ratios, and variability in $^{238}U/^{235}U$ ratios like modern-day AOC, reflecting seawater alteration of oceanic crust under oxygenated seawater conditions. In contrast, the 750 Ma ophiolite does not show the distinctive decreasing Th/U with increasing U concentrations trend of modern AOC and has fewer samples with $^{238}U/^{235}U$ ratios perturbed from mantle values, reflecting alteration under largely anoxic deep ocean conditions. This is also supported by Fe^{3+}/Fe_T ratios in these samples that are like unaltered modern MORB. Thus, our data suggest oxygenated deep oceans at some time between 750 and 540 Ma, either reflecting a full transition or intermittent deep ocean oxygenation events within an otherwise anoxic deep ocean.

Keywords

Uranium; Seawater alteration; Ophiolites; Altered oceanic crust; Deep Ocean oxygenation

1. Introduction

The evolution of the deep ocean redox state is important for Earth's surface biogeochemical cycles and the evolution of life (e.g., Holland, 1984; Canfield, 1998; Planavsky et al., 2011; Lyons et al., 2014, 2021, 2024 and references therein). Evidence points to the development of an oxic deep ocean in the late Proterozoic – early Phanerozoic (~ 850 to 400 Ma) in response to the rising abundance of oxygen in the atmosphere (Canfield et al., 2007, 2008; Scott et al., 2008; Dahl et al., 2014; Lyons et al., 2014; Sperling et al., 2015; Sahoo et al., 2016; Krause et al., 2018, 2022; Stockey et al., 2024). The atmospheric O_2 abundance needed to oxygenate the deep oceans is uncertain and estimates range from 15 to 50 % of present atmospheric levels (Canfield et al., 2007; Canfield, 2014; Stockey et al., 2024).

Estimates of deep ocean oxygen abundances through the late Proterozoic – early Phanerozoic are largely based on elemental and isotopic proxies (such as C, Fe, U, Mo, Cr, Zn) from sediments on continental shelfs and slopes. Studies on different locations and proxies have often resulted in differing views / timings on when the deep oceans became oxygen rich (e.g., see reviews in Lyons et al., 2014, 2021, 2024; Robbins et al., 2016; Krause et al., 2018, 2022; Mills et al., 2023; Stockey et al., 2024). One potential reconciliation using evidence from multiple proxies is that rather than steady conditions, the deep oceans in this time period likely had considerable variability, with 'brief' (<10 million years) periods of 'ocean oxygenation events', that may have been global or region-specific, against a backdrop of anoxic deep oceans (e.g., Sahoo et al., 2016; Tostevin and Mills, 2020; Krause et al., 2022). For example U isotopic compositions of sediments point towards brief, punctuated levels of deep ocean oxygenation in the Proterozoic, potentially as far back as 1000 Ma (e.g., Wei et al., 2021; Chen et al., 2022; Dang et al., 2022).

However, recent work from Stockey et al. (2024), using global compilations of U and Mo concentrations in shales and marine biogeochemical signals, infer an increase in atmospheric O_2 abundance at the Neoproterozoic – Palaeozoic boundary, but not by enough to oxygenate the deep oceans. Large changes in deep ocean conditions from anoxic / suboxic to more oxic conditions are not inferred until 539 to 400 Ma, with potential full deep ocean oxygenation comparable to modern-day at ~ 420 Ma (Stockey et al., 2024). Many of the proxies used for these estimates however represent local rather than global changes and are largely more representative of the shallower surface level oceans due to being based on sedimentary records. The debate over the timing of this critical change of Earth's surface environment encourages development of new archives of deep ocean conditions and redox-sensitive, elemental and isotopic tracers to probe them.

One novel, potentially more direct proxy of deep ocean redox conditions, is the alteration history of ophiolites. Ophiolites are the remnants of ancient oceanic crust that were subsequently accreted to the continents and thus may preserve a record of deep ocean conditions from their interaction with seawater during alteration. Stolper and Keller (2018) and Stolper et al. (2022) used ophiolites for this purpose by tracking the Fe^{3+}/Fe_T (where Fe_T is total Fe) of their extrusive sections back to 3500 Ma. Circulation of oxygen-rich seawater through oceanic crust oxidises Fe^{2+} to Fe^{3+}, elevating Fe^{3+}/Fe_T. Values above modern unaltered MORB and back arc basin basalts (Fe^{3+}/Fe_T ~ 0.31) indicate the interaction of the ophiolite with oxygen-rich deep ocean waters. The data of Stolper and Keller (2018) and Stolper et al. (2022) suggest that consistently elevated Fe^{3+}/Fe_T are only apparent from the early Phanerozoic and possibly not widespread until late Palaeozoic (<420 Ma).

Other redox sensitive characteristics of altered oceanic crust (AOC) may similarly trace deep ocean oxygenation. A notable feature of the uppermost 500 m of modern AOC is its enrichment in U abundances, by up to an order of magnitude through low temperature interaction with seawater (Hart and Staudigel, 1982; Bach et al., 2003; Kelley et al., 2003). Uranium has two main redox states, reduced and water insoluble U^{4+} and oxidised and water soluble U^{6+} (Langmuir, 1978). After the onset of the first major rise in atmospheric pO_2 across the great oxygenation event (~ 2300 Ma), there would have been a new supply of U^{6+} to the oceans from oxidative continental weathering. However under anoxic marine conditions, the majority of this U would have been reduced and sequestered as U^{4+} complexes into sediments in shallow settings, leading to a low U concentration oceanic reservoir (e.g., Anderson et al., 1989; Klinkhammer and Palmer, 1991; Partin et al., 2013). Only once the oceans became fully oxygenated, would U be present in appreciable abundance in the deep seawater that alters the oceanic crust. Lower U removal rates in ocean basins with decreasing area of anoxic seafloor area, resulted in increasing U concentration of seawater. On the current ocean floor, the enrichment of AOC with seawater U is seen through a clear trend of increasing U concentrations and decreasing Th/U ratios in AOC relative to fresh MORB (Fig. 1a). This trend is seen in multiple sections of modern AOC, with different spreading rates, and modern ophiolites, e.g., Troodos (92 Ma) (Fig. 1a). Thorium is a useful comparison to U due to their similar magmatic behaviours, where both are typically present in the 4+ oxidation state, but different behaviours in the modern, oxidised surface environment, with U being oxidised and water soluble in contrast to Th that is water insoluble. Thorium abundances therefore show little change in the oceanic crust during seawater alteration. The association of high U concentrations with low Th/U ratios in AOC, relative to unaltered MORB, is indicative of U addition from oxygenated seawater to the oceanic crust (Fig. 1a).

The enrichment and redistribution of U in the oceanic crust during oxygenated seawater alteration is also linked to redox sensitive isotopic fractionation that results in AOC having heterogenous $^{238}U/^{235}U$ compositions. Samples of AOC have U isotopic compositions that are both heavier (higher $^{238}U/^{235}U$) and lighter (lower $^{238}U/^{235}U$) than unaltered MORB, as shown from oceanic drill core sites 801C (Pacific), 417/418 (Atlantic), and 1256D (Pacific) (Andersen et al., 2015; Noordmann et al., 2016; Andersen et al., 2024) (Fig. 1b). In the shallowest portions of AOC U addition is dominated by sorption of U^{6+} onto secondary mineral surfaces, such as Fe-oxyhydroxides, which favours lighter U isotopes. In deeper regions of AOC, where conditions become more reducing, seawater transported U^{6+} may undergo partial reduction to U^{4+}, which favours heavier U isotopes, and subsequent incorporation into secondary minerals such as calcite (Andersen et al., 2015, 2024). As the oceanic crust cools and moves off-axis, the overlying sediment package thickness increases, so oxidised seawater flow becomes more restricted, conditions become increasingly reducing and the average $^{238}U/^{235}U$ ratio of AOC increases due to partial reduction processes becoming dominant (Andersen et al., 2024). Some samples of AOC with low Th/U ratios and high U concentrations show $^{238}U/^{235}U$ ratios similar to modern seawater and MORB, likely representing conditions with quantitative U uptake, with little to no net isotopic fractionation (Andersen et al., 2024).

A deep ocean dominated by anoxic conditions, should result in a different behaviour of U during oceanic crust alteration. Firstly, seawater would have a much lower capacity for carrying U into the deep oceans and presumably most would be lost in shelf settings. This would strongly limit the magnitude of elemental U enrichment in AOC. Secondly, the main mechanisms of U incorporation and isotopic fractionation into modern AOC will operate differently under anoxic conditions; in reducing seawater oxic U^{6+} would not be stable and any U uptake into oceanic crust would occur with more quantitative U^{4+} uptake, resulting in limited

isotopic variability in AOC. Thus, identifying when in geological history AOC first shows notable U enrichment (with associated low Th/U ratios), and isotopic variability in U should indicate the onset of oxygen-rich deep oceans.

We apply these U elemental and isotopic proxies using measurements of ophiolite samples. We measure the U concentration, Th/U ratio, and natural U isotopic variations in sample sets from three ophiolites: 750 Ma Gabal Gerf, North Africa (Zimmer et al., 1995), 540 Ma Khantaishir, Mongolia (Gianola et al., 2019), and 480 Ma Annieopsquotch, Canada (Lissenberg et al., 2005), which span the time range suggested for the onset of deep ocean oxygenation.

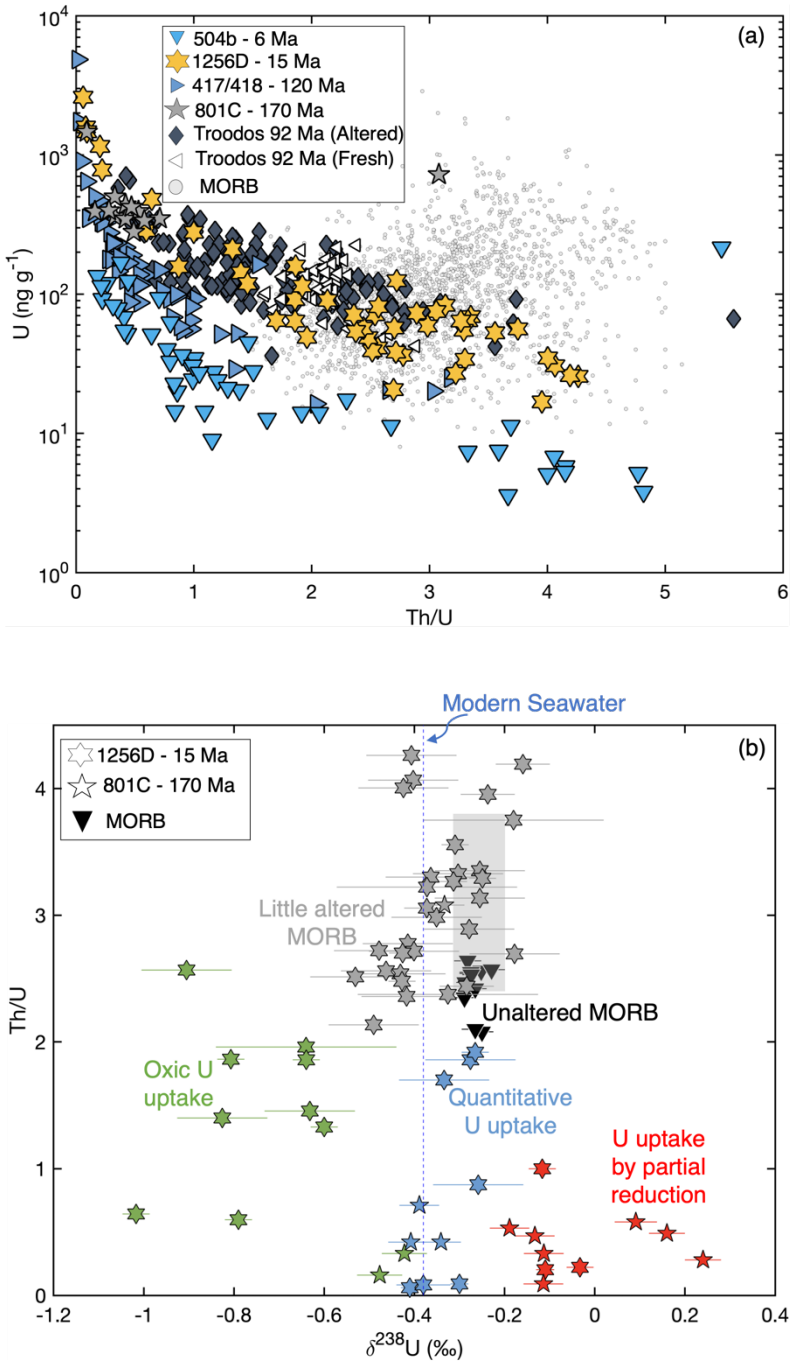

Fig. 1. (a) U concentration vs. Th/U ratio for AOC samples from the modern ocean floor: DSPD / ODP holes 504b (~ 6 Ma) (Bach et al., 2003), 1256D (~ 15 Ma) (Andersen et al., 2024), 417/418 (~ 120 Ma) (Seyedali et al., 2021), 801C (~ 170 Ma) (Andersen et al., 2015). Also shown are data for fresh (Regelous et al., 2014) and altered (Gillis et al., 2015) Troodos ophiolite (92 Ma) samples, and global MORB using a compilation of ICP-MS analyses from

Gale et al. (2013). (b) Th/U ratio vs. $\delta^{238}U$ for AOC samples from the modern ocean floor. Modern seawater composition (Kipp et al. 2022) is shown as a vertical blue dashed line. Grey shaded region represents the average Th/U of normal MORB ± 1 SD using a compilation of ICP-MS analyses from Gale et al. (2013), and the range in $\delta^{238}U$ for MORB (Andersen et al., 2015). Grey data points are samples that are closest in composition to fresh unaltered MORB (black, inverted triangles). Samples with lower Th/U imply U uptake during alteration but under different redox conditions: green data points are samples that are isotopically light (oxic U^{6+} adsorption), blue data points are samples that are similar to MORB or seawater in $\delta^{238}U$ and indicate quantitative U uptake, red data points are samples that are isotopically heavy (partial reduction of U^{6+} to U^{4+} and uptake). Note that DSDP site 417/418 (Noordmann et al., 2016) also has data for $\delta^{238}U$, however there are no associated Th/U values, so these samples are excluded from this figure. Error bars on $\delta^{238}U$ are 2SE.

2. Geological location and samples

The Annieopsquotch ophiolite, 480 Ma (U/Pb zircon age) (Dunning and Krogh, 1985) in Newfoundland, Canada is a 5.5 km thick section of oceanic crust, comprising gabbro, sheeted dykes, and basaltic pillow lavas, with hydrous mineralogical assemblages formed by seawater alteration (Lissenberg et al., 2005). Evidence of this includes dykes crosscutting hydrothermal alteration veins (Lissenberg et al., 2004) and a set of late-stage, off-axis dykes that crosscut the ophiolite stratigraphy that are markedly fresher than the host rocks (Lissenberg et al., 2005); neither would be the case if alteration occurred syn- or post-obduction as a metamorphic overprint (Lissenberg et al., 2005). The Annieopsquotch ophiolite formed following subduction initiation in the Iapetus Ocean and was accreted to the Laurentian continental margin within 10 Myr of formation (Lissenberg et al., 2005). Samples analysed in this work are from the sheeted dyke and extrusive sections.

The Khantaishir ophiolite in Western Mongolia, part of the Central Asian orogenic belt, is divided into the Naran and Taishir massifs, both with exposed mantle sections, overlain by gabbro, sill and dyke complexes, and pillow lavas. These have experienced limited greenschist-facies metamorphism that is either ocean floor or accretion related (Gianola et al., 2019) (with ocean floor alteration being favoured, see below). Reported ages for the Khantaishir ophiolite vary, with Sm-Nd ages of 532 ±40 Ma for the Taishir massif and 540 ±12 Ma for the Naran massif (Gianola et al., 2019), while U/Pb dating of plagiogranites suggests ages of 573 ±8 Ma and 566 ±7 Ma (Jian et al., 2014). Gianola et al., (2019) estimate an age range of ~ 550 – 530 Ma, and for this study, we use an average age of 540 Ma. Dating of metamorphic zircons from a shear zone at the ophiolite's boundary with the microcontinent it accreted to suggest

obduction occurred at 514 ±8 Ma (Jian et al., 2014). Samples analysed here span the gabbro, sill and dyke complex, and extrusive section.

The Gabal Gerf ophiolite, located in the Southern Eastern Desert of Egypt and Red Sea Hills of Sudan, is part of the Arabian-Nubian shield (Zimmer et al., 1995). It consists of the Gabal Gerf, Gabal Harga Zarga, and Gabal Heiani nappe complexes, which include, a serpentinised ultramafic melange, serpentinised or carbonated ultramafics, gabbro, sheeted dykes, and basaltic pillow lavas which have variably experienced up to greenschist-facies metamorphism (Zimmer et al., 1995). Pooled Sm-Nd ages suggest a mean age of ~ 750 Ma for gabbro crystallisation (Zimmer et al., 1995), with obduction occurring around ~ 715 Ma (Kröner et al., 1992). Samples analysed in this work cover ultramafic cumulates, gabbro, sheeted dyke complexes, and pillow lavas.

Many ophiolites are formed in suprasubduction zone environments, which may result in lower Th/U ratios and higher U concentrations than MORB, as seen in fresh glass samples from the Troodos ophiolite (Fig. 1a). However, these fresh samples do not show such marked enrichment in U concentration and low Th/U as most of their altered counterparts (Fig. 1a). Therefore, we emphasise that the tectonic setting of oceanic crust for each ophiolite has a minor influence on the magnitude of U enrichment, relative to the effect of seafloor alteration that dominates over any primary differences (Fig. 1a). Details on the tectonic settings of each ophiolite are, however, provided in Supplementary Material Section 1.

A full comparison of alteration mineralogy in modern AOC and our samples is beyond the scope of this work, but details can be found in other studies (e.g., Alt and Honnorez, 1984; Zimmer et al., 1995; Alt and Teagle, 2003; Lissenberg et al., 2004, 2005; Alt et al., 2010;

Gianola et al., 2019). However, we provide some descriptions and representative petrographic images illustrating the typical mineralogy of submarine alteration evident in the ophiolite samples in Supplementary Material: Section 1. In brief, low temperature alteration phases (e.g., celadonite, saponite, and prehnite), variations in mineralogy with seafloor temperature gradient (celadonite in extrusive section samples and calcite and epidote in deeper dyke samples), and primary igneous textures (e.g., ophitic and pilotassitic textures) are evident in Annieopsquotch and Khantaishir ophiolite samples (Fig. S2). This, in conjunction with field observations given above, indicate that the ophiolites preserve seafloor alteration characteristics rather than metamorphic overprints syn- or post-obduction. It is important to note that while the samples studied in this work were dominantly collected to study magmatic processes, and so the most seawater altered samples may have been systematically avoided, the alteration mineralogy identified and differences between more altered (Fig. S2a-e) and fresher samples (Fig. S2f), indicates heterogeneous alteration of samples, as would be expected from seawater alteration. We therefore consider our samples to be representative of submarine alteration of *in-situ* oceanic crust. Unfortunately, no thin sections were available for the Gabel Gerf samples.

3. Methods

Major and trace element data for the ophiolite samples are reported in Zimmer et al. (1995), Lissenberg et al. (2005), and Gianola et al. (2019). For measurement of Th and U concentrations (non-isotope dilution) 50 mg of sample powders were dissolved and analysed on a ThermoFinnigan Element2 at the Bristol Isotope Group laboratories following Andersen et al. (2014). Measured reference materials are in good agreement with reference values (Supplementary Material: Section 2).

Uranium isotopic measurement, sample preparation and analysis followed Andersen et al. (2015), detailed fully in Supplementary Material: Section 2. Uranium isotope analysis was conducted in the University of Bristol Isotope Group laboratories. Approximately 0.5 – 3 g of sample powder, spiked with the IRMM3636 ^{236}U – ^{233}U double spike (Richter et al., 2008), was dissolved. Purification and U separation used a two-column method, with TRU resin followed by UTEVA resin. Uranium aliquots were dissolved in 0.2 M HCl (aiming for U concentrations of 50 – 300 ng g^{-1}) for isotopic analysis. Procedural blanks were <30 pg U, negligible compared to amount of U consumed per measurement, ~ 15 – 80 ng.

Uranium isotope compositions were measured on a ThermoFinnigan Neptune MC-ICP-MS (serial no. 1002) in low mass resolution ($M/\Delta M$ ~ 2000, 5 to 95 % peak height definition). Samples were bracketed by measurements of the double-spiked standard CRM-145. Uranium isotope ratios for $^{238}U/^{235}U$ and $^{234}U/^{238}U$ were calculated using the exponential mass fractionation law and reference double spike $^{233}U/^{236}U$ ratio (Richter et al., 2008). Data are reported in δ notation with $\delta^{238}U = [(^{238}U/^{235}U_{Sample} / {}^{238}U/^{235}U_{CRM\text{-}145}) - 1]$ and $\delta^{234}U = [(^{234}U/^{238}U_{Sample} / (^{234}U/^{238}U_{CRM\text{-}145}/ (1–0.0386)) - 1]$. Note that $\delta^{234}U$ values are reported

relative to secular equilibrium, given the CRM-145 standard has a $\delta^{234}U$ of −38.6 ‰ relative to secular equilibrium (Cheng et al., 2013).

Long term external reproducibility at various measured U intensities has been estimated using aliquots of the well characterised reference material BHVO-2 measured during different analytical sessions. The external reproducibility of $\delta^{238}U$ and $\delta^{234}U$ for BHVO-2 ranges from ±0.09 – 0.03 ‰, 2SD, and ±4 – 0.9 ‰, 2SD, respectively, for measured ^{238}U intensities of 200 – 1000 pA respectively (full details reported in Supplementary Material: Section 2). Uranium isotopic measurements of international reference materials analysed (BHVO-2, BCR-2, BIR, W-2A, and CZ1) agree with literature values (Supplementary Material: Section 2).

4. Results

Uranium isotopic compositions, concentrations, and Th/U ratios are reported in Supplementary Material: Section 3 and table S3. To present a homogeneous dataset, we exclude from further discussion: 1) samples measured for Th/U ratios, but not U isotopic compositions and 2) amphibolites and ultramafic / peridotite samples that have undergone serpentinization from Gabel Gerf, given these lithologies are not represented in the other ophiolites, Moreover, Pavia et al. (2023) illustrated the latter are sensitive to post-serpentinization weathering processes in subaerial environments that question their utility as palaeo-seawater archives.

Some samples from Annieopsquotch (480 Ma) and Khantaishir (540 Ma) show enrichment in U relative to Th, with high U concentrations and low Th/U ratios relative to the field defined by MORB (Fig. 2a, b). This trend of simple U-addition is similar to that seen in modern sections of AOC the Troodos ophiolite (Fig. 2b). In figures, we highlight the samples that plot on this vector of U enrichment relative to modern MORB associated with decreasing Th/U ratios, as observed in AOC in the current ocean basins. Such samples are identified as having Th/U ratios lower than one standard deviation of average MORB Th/U from spreading centres and back arc settings, i.e., a Th/U ratio <2.4, using a compilation of ICP-MS analyses from Gale et al. (2013), and U concentrations above 55 ng g^{-1}, the average concentration of depleted MORB from Gale et al. (2013). Nine samples from Khantaishir and five from Annieopsquotch pass these criteria and define a similar array to data from modern AOC and altered Troodos ophiolite samples (Fig. 2a & b). In contrast, Gabel Gerf (750 Ma) samples, which generally have lower Th concentrations (Fig. 2a), have low Th/U ratios in samples that also have low U concentrations (Fig. 2b).

Samples from all three ophiolites have $\delta^{238}U$ that overlap with MORB (Fig. 2c). However, samples with low Th/U ratios from Annieopsquotch and Khantaishir, and a single sample from Gabel Gerf, have $\delta^{238}U$ lower than fresh MORB, similar to modern AOC (Andersen et al., 2015, 2024). There are no $\delta^{238}U$ measurements, outside of uncertainty, higher than the field of modern MORB (Fig. 2c).

Samples from all ophiolites show variation in $\delta^{234}U$ with compositions above and below secular equilibrium, where secular equilibrium is $\delta^{234}U = 0$ (Fig. 3). However, most samples have $\delta^{234}U > 0$ and extend up to ~ +442 ‰, above modern seawater (145.6 ±0.3 ‰, 2SE; Kipp et al., 2022). There are no clear correlations between $\delta^{234}U$ and $\delta^{238}U$ or U concentrations (Fig. 3a & b) or Th/U ratios (Fig. S4). In general, however, samples with the lowest U concentrations tend to have the greatest deviation in $\delta^{234}U$ from secular equilibrium (Fig. 3b). This overview excludes the anomalous Khantaishir sample with the highest $\delta^{234}U$ (~ +442 ‰) that also has a high U concentration (~ 183 ng g^{-1}), marked with a cross on figures 2 and 3.

Figures 2 and 3 distinguish samples by lithology, which provides a coarse index of depth within the ophiolite stratigraphy. Samples with the highest U concentrations and values of $\delta^{238}U$ lower than MORB are predominantly, but not exclusively, from the extrusive sections of ophiolites (Fig. S5). This also argues against post-obduction alteration of samples, which would result in all sections showing similar degrees of alteration.

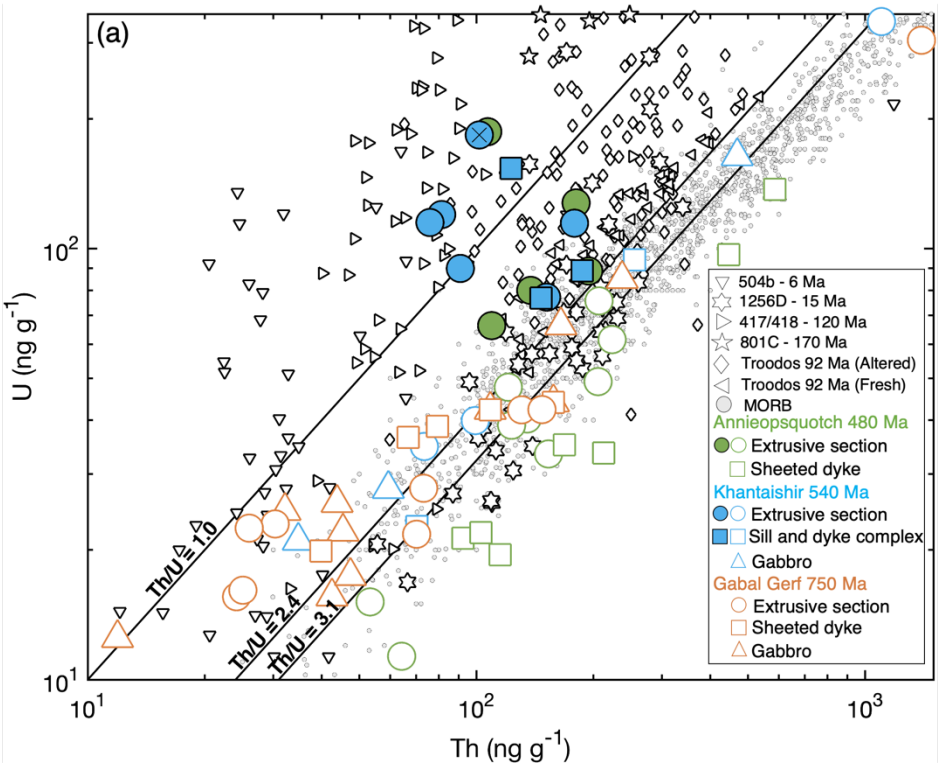
(a)
U (ng g-1)
Th (ng g-1)
Th/U = 1.0
Th/U = 2.4
Th/U = 3.1
504b - 6 Ma
1256D - 15 Ma
417/418 - 120 Ma
801C - 170 Ma
Troodos 92 Ma (Altered)
Troodos 92 Ma (Fresh)
MORB
Annieopsquotch 480 Ma
Extrusive section
Sheeted dyke
Khantaishir 540 Ma
Extrusive section
Sill and dyke complex
Gabbro
Gabal Gerf 750 Ma
Extrusive section
Sheeted dyke
Gabbro

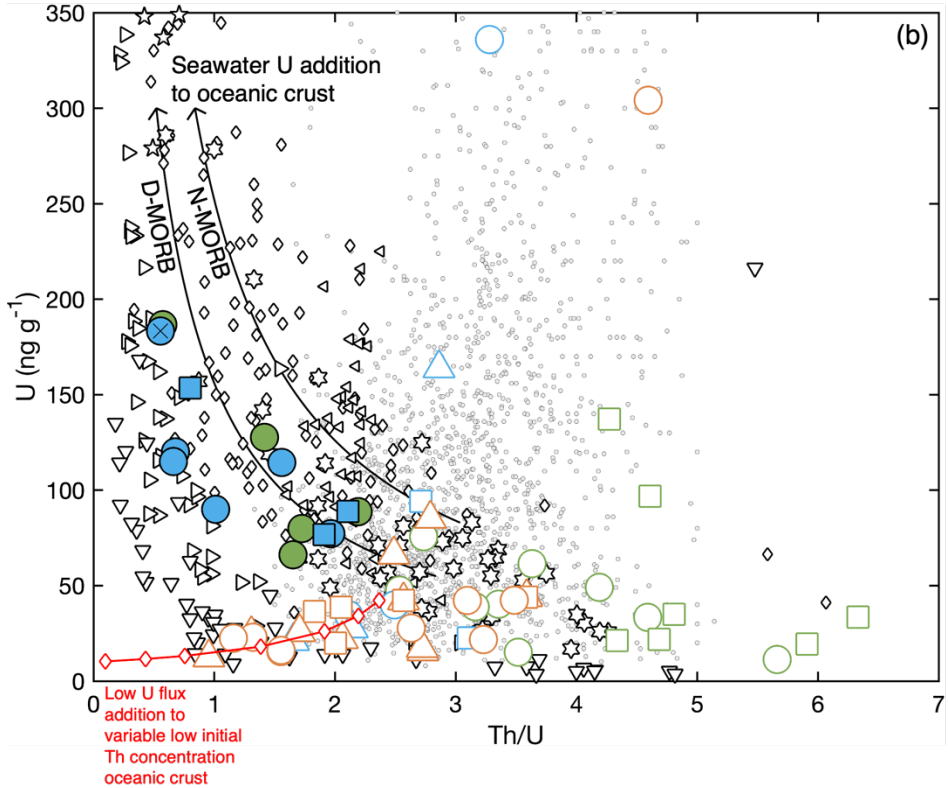
(b)
Seawater U addition
to oceanic crust
D-MORB
N-MORB
U (ng g-1)
Th/U
Low U flux
addition to
variable low initial
Th concentration
oceanic crust

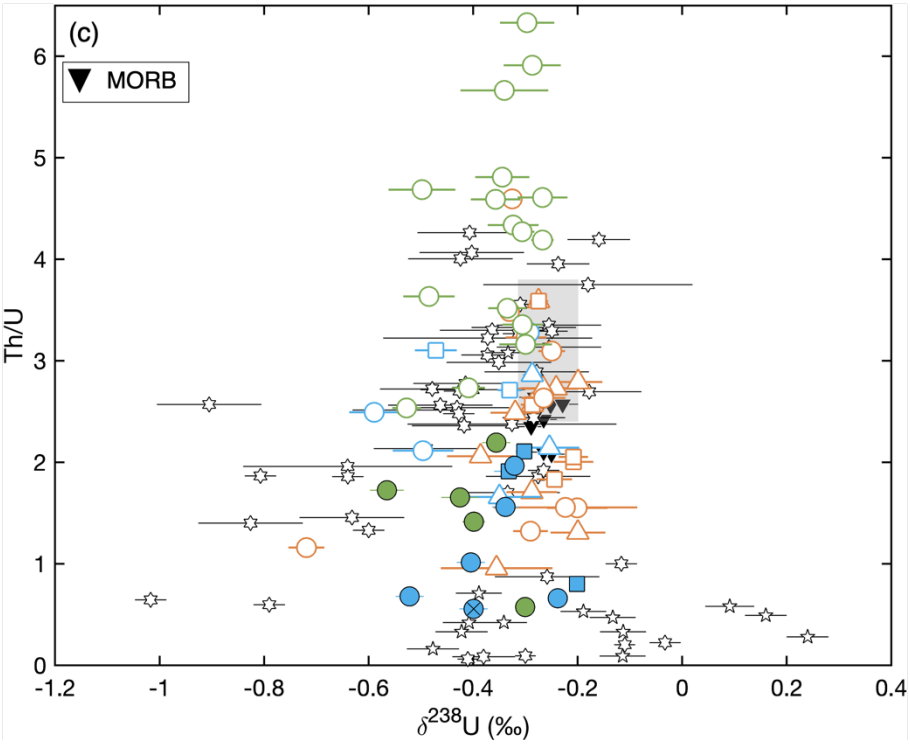

Fig. 2. (a) U concentration vs. Th concentration, (b) U concentration vs. Th/U ratio and (c) Th/U ratio vs. δ^{238}U for ophiolite samples, modern sections of AOC, the Troodos ophiolite, and MORB. Symbols are the same as in figure 1. Ophiolite data are grouped into lithology of samples, circles are samples from the extrusive section, squares are sheeted dykes / sill and dykes, and triangles are gabbros. Green samples are from Annieopsquotch, blue from Khantaishir, and orange from Gabal Gerf. Ophiolite samples are grouped into two sets, those that plot on a vector of U addition to MORB and have increasing U concentration and decreasing Th/U indicative of U addition from typical MORB compositions (filled symbols) and those that do not (hollow symbols), see (b) and main text for details. The Khantaishir sample with the highest δ^{234}U (Fig. 3a) is marked with a cross. In (a) three lines of constant Th/U, 3.1 (average MORB), 2.4, and 1 are shown. Note that

464 the concentrations are on a log scale and have been cut at concentrations of Th
465 1500 ng g^{-1} and U 350 ng g^{-1}. In (b) two representative mixing curves (black lines)
466 show the effect of simple U addition to a normal and depleted MORB starting
467 composition from Gale et al. (2013). Also, in (b) the red line denotes oceanic crust
468 compositions with variable low initial Th concentrations (white diamonds at 100,
469 75, 50, 25, 10, 5, and 1 ng g^{-1} Th) and constant Th/U ratio of 3.1 that has been
470 perturbed by a representative equal amount of a low U flux, 10 ng g^{-1}. In (c) Error
471 bars on $\delta^{238}U$ are 2SE.

472

473

474

475

476

477

478

479

480

481

482

483

484

485

486

487

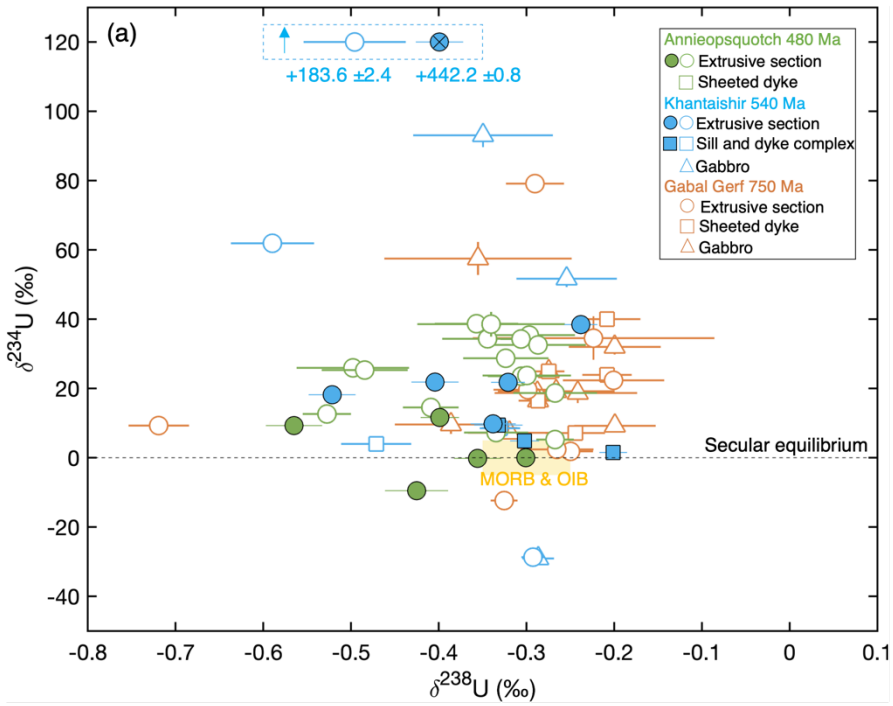
(a)
+183.6 ±2.4
+442.2 ±0.8
Annieopsquotch 480 Ma
Extrusive section
Sheeted dyke
Khantaishir 540 Ma
Extrusive section
Sill and dyke complex
Gabbro
Gabal Gerf 750 Ma
Extrusive section
Sheeted dyke
Gabbro
Secular equilibrium
MORB & OIB
δ234U (‰)
δ238U (‰)

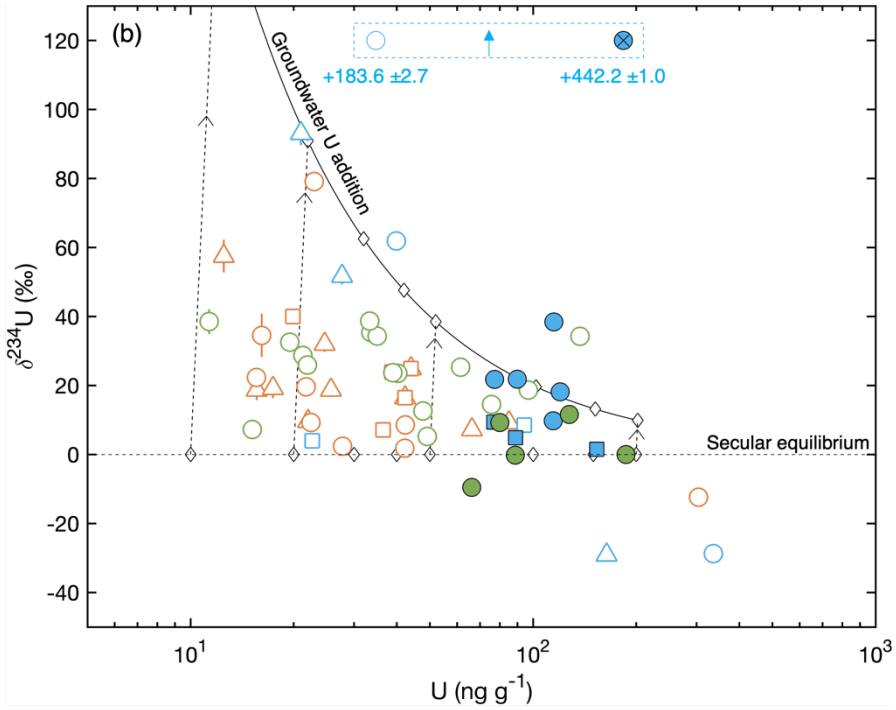
(b)
+183.6 ±2.7
+442.2 ±1.0
Groundwater U addition
Secular equilibrium
δ234U (‰)
U (ng g-1)

Fig. 3. (a) $\delta^{234}U$ vs. $\delta^{238}U$ and (b) $\delta^{234}U$ vs. U concentration for ophiolite samples. Dashed black line at $\delta^{234}U = 0$ represents secular equilibrium. Ophiolite sample symbol groupings shapes, and colours are the same as in figure 2. Samples from Khantaishir circled in the dashed blue box plot off the scale in $\delta^{234}U$ (Table S3). In (a) the yellow shaded region is the range of $\delta^{234}U$ and $\delta^{238}U$ represented by MORB and ocean island basalt (OIB) samples from Andersen et al., (2015). In (b) the result of addition of a constant flux of groundwater U (2 ng g^{-1} with $\delta^{234}U = 1000$ ‰) to samples in secular equilibrium, with a range of initial U concentrations, is shown as the solid black curved line. Vectors of alteration (dashed lines) link specific fresh and altered hypothetical samples (white diamonds) with initial U concentrations (10, 20, 30, 40, 50, 100, 150, and 200 ng g^{-1}). Note that in (b) the U concentration is plotted on a log scale. Error bars are 2SE.

5. Discussion

5.1 Secular equilibrium and sample alteration

The U budgets of ophiolites represent the primary rock inventory with additions from ancient seafloor alteration and possibly more recent subaerial exposure. Measurements of $\delta^{234}U$ can help differentiate these processes. A deviation from secular equilibrium ($\delta^{234}U = 0$) suggests U loss or gain in the last ~ 2 Myr. Uranium loss during chemical weathering typically causes ^{234}U deficits ($\delta^{234}U < 0$) through preferential loss of daughter ^{234}U atoms that sit in damaged recoil sites (Thurber, 1962; Bacon, 1978; MacDougall et al., 1979; Chabaux et al., 2003; Gaschnig et al., 2021) resulting in complementary $\delta^{234}U > 0$ of decreasing magnitude in groundwaters, rivers, and oceans (e.g., Osmond and Cowart, 1976; Dunk et al., 2002; Kipp et al., 2022).

Many samples measured across all three ophiolites, have $\delta^{234}U$ higher than secular equilibrium, implying some recent U gain. In subsurface aqueous environments equilibrium adsorption-desorption exchange between ionic U^{6+} complexed species in the groundwater and mineral surfaces can lead to net adsorptive U uptake (e.g., Osmond and Cowart, 1976; Sylwester et al., 2000). The extreme $\delta^{234}U$ of groundwater, typically ~ 50 – 1000 ‰ (extending to >2000 ‰) (Osmond and Cowart, 1976), means samples can acquire modestly perturbed $\delta^{234}U$ (~ 20 ‰) with only minor elemental U addition. We illustrate this in figure 3b where hypothetical samples with a range of initial U concentrations (white diamonds at secular equilibrium) are perturbed by a fixed addition of groundwater U (2 ng g^{-1} with a characteristic $\delta^{234}U$ value of 1000 ‰). This yields the black curve (perturbed samples shown as white diamonds along this curve, which are shifted imperceptibly along the x-axis i.e., minor total U addition) that reproduces much of the variability seen in $\delta^{234}U$, including the tendency for samples with lower

U concentration to have higher $\delta^{234}U$. For samples with U concentrations over 20 ng g^{-1} this flux would account for <10 % of the U content of samples, this would result in a small shift in U concentrations. We also, following the approach in Andersen et al. (2024), model the changes in Th/U ratios (Fig. S6a) and $\delta^{238}U$ (Fig. S6b & c) following groundwater U addition with $\delta^{234}U$ = 1000 ‰ (Supplementary Material: Section 4). In brief shifts in Th/U and $\delta^{238}U$ are calculated and to account for unknown $\delta^{238}U$ compositions of groundwater we model two scenarios using the lowest and highest $\delta^{238}U$ compositions in each ophiolite for the groundwater composition. We assume starting $\delta^{234}U$ compositions of 0 ‰ for the rock with no groundwater U addition and apply the model to samples with $\delta^{234}U \geq 0$ ‰. Samples plot within uncertainty of a 1:1 line between corrected compositions for groundwater U addition and the measured compositions in Th/U and $\delta^{238}U$ (Fig. S6), except for the sample from Khantaishir with highest $\delta^{234}U$ (~ 44 % groundwater U addition, Table S4). This sample, however, when corrected for recent U addition still shows evidence of seawater U addition, i.e., low Th/U (measured Th/U 0.6 versus corrected Th/U 1.0). This simple model highlights that recent subaerial weathering may not have a significant impact on Th/U and $\delta^{238}U$ compositions, even when showing elevated $\delta^{234}U$.

An important observation is also that samples with high U concentrations are not systematically associated with elevated $\delta^{234}U$. This indicates that alteration during recent ophiolite exposure is not the main cause of their U enrichment relative to MORB. The $\delta^{234}U$ isotopic data however only preserve the last ~ 2 Myr of groundwater interaction and therefore do not reflect the entire history of potential groundwater U addition that may have occurred over longer timescales. As discussed above, however, other lines of evidence, such as the alteration mineralogy of samples indicating seafloor alteration assemblages rather than subaerially formed secondary minerals, support the inference of limited groundwater U addition to the samples.

Furthermore, there is no obvious relationship between $\delta^{234}U$ and $\delta^{238}U$ (Fig. 3a). Much of the range of $\delta^{234}U$ is found in samples with $\delta^{238}U$ within uncertainty of primary magmatic $\delta^{238}U$ (Fig. 3a). This supports the notion developed above that modest perturbation of $\delta^{234}U$ by groundwaters with high $\delta^{234}U$ need not dramatically alter the overall U budget, especially for samples with high U concentrations from submarine alteration acquired before such subaerial weathering (Fig. S6). The low U concentrations of groundwater (e.g., Dunk et al., 2002) results in only minor amounts of U addition compared to the greater quantities of U that may be added by larger volumes of U-rich seawater during seafloor alteration. Therefore, our samples may have experienced recent subaerial groundwater U addition, but, and especially for samples with high U concentrations, this would not result in significant changes in U elemental and isotopic compositions, although larger changes may occur in low U concentration samples. We therefore focus our interpretations on high U concentration samples with low Th/U ratios that are most indicative of compositions resulting from seafloor alteration.

5.2 Comparisons of ophiolites to more recent altered oceanic crust

Our analyses show distinct patterns of U enrichment in the two younger ophiolites relative to the oldest one. In the former, most samples with high U concentrations plot on a vector of increasing U concentration and decreasing Th/U ratio, similar to modern AOC (Fig. 2b). This trend is readily explained by the process of U addition during seafloor alteration, which we depict on figure 2b (Hart and Staudigel, 1982; Bach et al., 2003; Kelley et al., 2003; Andersen et al., 2015, 2024). Some Annieopsquotch samples extend to high Th/U ratios (>4.5) at low U concentrations (Fig. 2a, b) which may indicate some U loss and or remobilisation as seen in some deeper sections of modern AOC (Andersen et al., 2024).

612

613 Samples from the older Gabel Gerf ophiolite also have Th/U ratios lower than unaltered
614 MORB, but in samples with the lowest rather than the highest U concentrations (Fig. 2b). They
615 define a group with low Th and U concentrations, distinct from the Khantaishir and
616 Annieopsquotch samples that show significant U enrichment similar to modern seafloor
617 samples (Fig. 2a). The variable but low Th/U ratios in Gabal Gerf likely reflect the addition of
618 small amounts of seawater or recent groundwater U to oceanic crust with low initial Th
619 concentrations (Fig. 2a & b), orders of magnitude smaller than that observed in Khantaishir,
620 Annieopsquotch, and modern AOC. We reproduce these Gabel Gerf samples with a simple
621 model that starts with a range of unaltered crustal compositions with variable, low initial Th
622 concentrations (1, 5, 10, 25, 50, 75, and 100 ng g^{-1}) but constant Th/U ratios (3.1). A fixed,
623 low U flux (10 ng g^{-1}) added to these model compositions successfully accounts for the trend
624 displayed by the Gabal Gerf and some Khantaishir samples, that have low Th/U ratios (Fig.
625 2b) and low Th and U concentrations (Fig. 2a). There are no Gabel Gerf samples that plot on
626 vector of seawater U addition to oceanic crust, with low Th/U ratios at high U concentrations
627 (Fig. 2b). The systematics of U and Th trends identified in the Gabal Gerf samples are therefore
628 not characteristic of seawater alteration on the modern, oxic ocean floor. They are more readily
629 attributed to minor U addition, from either groundwater of perhaps more simply, from seafloor
630 alteration in an anoxic ocean. The Gabal Gerf data therefore suggest that the redox state of the
631 deep oceans was different at ~ 750 Ma relative to 540 and 480 Ma.

632

633 The contrast in the $\delta^{238}U$ between the oldest and more recent ophiolites is more subtle than the
634 contrast in U concentrations and Th/U ratios. All analyses of Gabel Gerf, bar one sample, are
635 within error of modern magmatic $\delta^{238}U$ (Fig. 2c). As argued above, the low Th/U ratio in some
636 Gabel Gerf samples reflect minor U addition to low Th concentration samples. This process

637 appears to result in perturbed $\delta^{238}U$ in only one case, with this sample also having a low U
638 concentration (Fig. S5) and may be related to recent groundwater U addition. All other Gabal
639 Gerf samples reflect the unfractionated bulk addition of minor amounts of U, which we
640 attribute to this process occurring in an anoxic ocean. In contrast, $\delta^{238}U$ in some low Th/U ratio
641 samples from both Khantaishir and Annieopsquotch are significantly lower than unaltered
642 modern MORB (Fig. 2c), which we interpret as further evidence of oxic submarine alteration.
643 This is a less definitive signature than the U-Th elemental systematics, as different styles of
644 ^{238}U-^{235}U fractionation are observed with depth in modern AOC (Andersen et al., 2015, 2024).
645 In keeping, some of the low Th/U ratio samples from Khantaishir and Annieopsquotch have
646 $\delta^{238}U$ within uncertainty of unaltered MORB, likely reflecting near-quantitative U addition
647 during seafloor alteration.
648
649 It is notable that there are no $\delta^{238}U$ compositions outside of uncertainty in the ophiolite samples
650 higher than unaltered MORB, as can occur through partial reduction of U^{6+} (Fig. 1b). Altered
651 oceanic crust may develop high $\delta^{238}U$ from more restrictive U addition due to sediment build
652 up off-axis restricting the flow of oxidised seawater through the oceanic crust. Conditions of
653 alteration therefore can become more reducing with age of oceanic crust, resulting in higher
654 $\delta^{238}U$, as seen in some modern AOC, most notably from the oldest AOC samples (Hole 801,
655 Fig. 1b) (Andersen et al., 2015, 2024). Our U enriched ophiolite samples may not have been
656 on the seafloor for long enough before obduction for conditions of alteration to become
657 dominantly reducing. As seen in hole 1256D (~ 15 Ma) the majority of samples have low $\delta^{238}U$
658 values, with high $\delta^{238}U$ only seen in a few samples at select horizons (Andersen et al., 2024).
659 Therefore, it is perhaps expected that most samples from AOC altered in an oxic deep ocean
660 analysed will have predominantly low $\delta^{238}U$ as is seen in Annieopsquotch and Khantaishir
661 ophiolite samples. Whether $\delta^{238}U$ values of AOC are higher or lower than MORB, our

conclusions remain unchanged, as both require that U^{6+} is present in the oxic deep oceans. The $\delta^{238}U$ data therefore corroborates with the inference from the elemental U and Th systematics of changing styles of submarine alteration from anoxic at 750 Ma to oxic at 540 and 480 Ma.

Comparisons of ophiolite samples with modern AOC are potentially affected by sampling biases, as ophiolite samples are typically collected to study magmatic processes and so the most seawater altered samples may be avoided. This could explain some of the more muted levels of U enrichment seen in our samples from Khantaishir and Annieopsquotch and the lack of enrichment seen in Gabal Gerf. In this context we note that our interpretation of Gabal Gerf as altered in anoxic deep ocean conditions is a conservative interpretation. If the lack of U enrichment at Gabal Gerf were solely due to a sample bias, then it would extend our inferred duration of oxic deep ocean conditions considerably further back in time than most current estimates (see section 1 and 5.3). Thus, the lack of U enrichment in Gabal Gerf is unsurprising. More significant is the evidence for U addition in Khantaishir samples, indicative of oxic deep oceans at 540 Ma, also older than many literature estimates.

5.3 Comparison with other recent models of changing ocean anoxia

Given the use of ocean crust alteration recorded in ophiolites in this study, it is valuable to compare our observations to the estimates of deep ocean dissolved O_2 concentrations derived from Fe^{3+}/Fe_T ratios in ophiolites (Stolper and Keller 2018). Stolper and Keller (2018) calculate a gradual increase in the dissolved O_2 concentration of the deep ocean from anoxic conditions in the Neoproterozoic (a period encompassing the Gabel Gerf ophiolite) to values resolvable from zero in the early Palaeozoic (during which Annieopsquotch and Khantaishir were formed and altered), with subsequent continued rise to modern day concentrations (Fig. S7a). We note

687 that the Fe^{3+}/Fe_T ratios of Gabal Gerf samples are amongst the most reduced values in the
688 Neoproterozoic time step of Stolper and Keller (Fig. S7b) and Fe^{3+}/Fe_T in Gabal Gerf samples
689 show no correlation with $\delta^{238}U$ (Fig. S8). Unfortunately, we do not have Fe^{3+}/Fe_T data for our
690 Annieopsquotch or Khantaishir samples.
691
692 The systematic change in style of seawater U addition between ophiolites of different ages in
693 our study is, at least qualitatively, consistent with the timing of onset of discernible deep ocean
694 oxygenation inferred by Stolper and Keller (2018). However, their model does not show a
695 significant rise in deep ocean O_2 concentrations until ~ 420 Ma, which is younger than the
696 formation and obduction of our youngest ophiolite (480 Ma) which we infer to have
697 experienced alteration in an oxygenated deep ocean. In a subsequent, more detailed study of
698 the Bay of Island ophiolite (485 Ma) Stolper et al. (2022) infer, from Fe^{3+}/Fe_T ratios, oxidation
699 of volcanic rocks in the ophiolite sequence, but to less of an extent than seen in the late
700 Palaeozoic-modern systems. Stolper et al. (2022) argue that, from globally binned averages,
701 the clear increase in deep ocean O_2 is not seen until the late Palaeozoic. However, with
702 individual locations (e.g., Bay of Island, Annieopsquotch, Khantaishir), increases in deep ocean
703 O_2 can be seen earlier, which may represent a global trend or local / transient events in deep
704 ocean O_2 levels. It is encouraging that Annieopsquotch and the Bay of Island ophiolite, both of
705 similar ages and from similar palaeo-geographic locations show evidence of increased deep
706 ocean O_2 from different palaeo-redox proxies.
707
708 Perfect agreement between the two proxies is not expected however, as the controls on Fe
709 oxidation and U addition through seawater interaction are different and redox thresholds
710 between the systems may be different. The main host minerals and sites for U in AOC are
711 poorly constrained and U addition may be associated with multiple phases of secondary

712 mineral formation in oxidising and reducing conditions. Increases in Fe^{3+}/Fe_T ratios however,
713 that may scale with increasing levels of deep ocean O_2, will primarily be associated with phases
714 such as Fe-oxyhydroxides that may overprint earlier alteration phases (Alt, 2004). Uranium
715 addition to AOC, which may not directly scale with increasing levels of deep ocean O_2, may
716 be more sensitive to low levels of dissolved O_2 than Fe^{3+}/Fe_T ratios. Different elemental
717 systems have different thermodynamic redox thresholds, however, the exact redox potential for
718 each element will vary as a function of the local chemical and physical conditions (e.g., pH
719 and ligand-complexation) and lithology investigated (Langmuir, 1978; Anderson et al., 1989;
720 Algeo and Li, 2020). Therefore, the measurable fingerprint of deep ocean oxygenation may
721 differ for the U and Fe system during seafloor alteration in AOC. Our U data could record
722 lower levels of deep ocean oxygenation than recorded by the Fe system (Stolper and Keller,
723 2018; Stolper et al., 2022), thus providing a potential explanation for the different time
724 inferences from the proxies. Overall, however we stress that it is difficult to envisage the
725 extensive addition of U to the oceanic crust, which we observe in 480 and 540 Ma ophiolites,
726 without high U concentration in deep ocean water, which requires an oxygenated deep ocean.
727
728 Sedimentary records have also been analysed to investigate deep ocean O_2 (see section 1) and
729 the marked rise in U content in some marine sedimentary sections at ~ 600 Ma (e.g., Partin et
730 al., 2013) has been interpreted to reflect the timing of deep ocean oxygenation, similar to the
731 timing based on arguments from the diversification of life (e.g., Butterfield, 2007; Canfield et
732 al., 2007; Dahl et al., 2010; Lenton et al., 2014; Planavsky et al., 2014). However, a recent
733 compilation of marine sedimentary U and Mo concentration data, suggests no major change in
734 the oxygen content of the deep oceans until ~ 420 – 400 Ma (Stockey et al., 2024). This timing
735 again is significantly later than our inference of deep ocean oxygenation >540 Ma.
736

A possible explanation of the different inferred timing of deep ocean oxygenation is that the approaches have a different sensitivity to transient ocean oxygenation events, i.e., brief periods of increased ocean oxygenation against a backdrop of long term ocean anoxia. Marine sedimentary data integrates over ~ 10-million-year timescales, and as such, may not capture transitory ocean oxygenation events. Although ophiolites also integrate conditions on the deep ocean floor over a similar timescale, a signature of U addition from a short-lived period of oxygenation can be seen as an elevated U concentration or low Th/U ratio relative to a baseline of unaltered MORB. In the sedimentary case, short-lived periods of oxygenation, that result in spikes in U concentrations relative to average compositions, may be damped by the averaging effect of continuous sedimentation. Thus, it may be that the U ophiolite proxy is better at capturing shorter ocean oxygenation events in an otherwise anoxic deep ocean.

However, ophiolites provide a direct record of interaction between basaltic rock and deep ocean water, while sedimentary proxies of ocean anoxia trace local conditions on continental shelves and the consequences of these observations for deep ocean conditions requires further biogeochemical modelling. It is interesting to note that the raw sediment U concentration data in the study of Stockey et al. (2024, their supplementary Fig. S2) show a systematic increase in the 75th percentile and maximum value in temporally binned samples younger than ~ 550 Ma. Only with a more sophisticated, statistical learning treatment, to address sample bias, is the rise in sedimentary U content (used to model oxygenation of the deep ocean) delayed until ~ 420 – 400 Ma.

6. Conclusions

Mafic samples from the Annieopsquotch (480 Ma) and Khantaishir (540 Ma) ophiolites showing a trend between low Th/U ratios, <2.4, and high U concentrations, >55 ng g^{-1}, and variability in $\delta^{238}U$, ranging from –0.5 to –0.2 ‰, reflect the significant uptake of U during seafloor alteration prior to obduction. These observations imply alteration by oxic, deep ocean water, with U present in its oxidised form, since at least 540 Ma. Samples from the Gabal Gerf 750 Ma ophiolite do not show this systematic significant deep ocean U addition and likely reflect seawater alteration of ocean crust under anoxic conditions. The Th-U elemental, and U isotopic compositions of Gabal Gerf are consistent with Fe^{3+}/Fe_T ratios of the samples, that reflect anoxic alteration conditions. Our data argue for deep ocean oxygenation between 750 – 540 Ma, but it is not clear if the ophiolite data reflect a full transition or intermittent events within a largely anoxic deep ocean. Nonetheless, U abundances and Th/U ratios of ophiolites are useful tracers of the oxygenation state of deep ocean water during its alteration of the oceanic crust. The U isotope data, that suggest ^{238}U-^{235}U isotopic fractionation during U uptake into ancient AOC similar to processes in modern AOC, provide important supporting information but are less diagnostic given the relatively small isotopic fractionations and ability of different styles of seafloor alteration to cause fractionations in different senses.

Credit authorship contribution statement

Joel B. Rodney: Data curation, formal analysis, investigation, methodology, validation, visualisation, writing – original draft. **Morten B. Andersen:** Supervision, project administration, funding acquisition, conceptualization, methodology, writing – review and editing. **Daniel Stubbs:** Methodology, writing – review and editing. **C. Johan Lissenberg:** Resources, writing – review and editing. **Omar Gianola:** Resources, writing – review and editing. **Matthias Willbold:** Resources, writing – review and editing. **Tim Elliott:** Supervision, project administration, funding acquisition, conceptualization, writing – review and editing.

Declaration of competing interest

The authors declare that they have no known competing financial interests or personal relationships that could have appeared to influence the work reported in this paper.

Data availability

Data are available through Mendeley data at:

https://data.mendeley.com/datasets/fyk72sg4km/4

Acknowledgments

JBR would like to acknowledge Christopher D. Coath and Carolyn Taylor for the upkeep of the labs. JBR would like to acknowledge Ian Parkinson, Paul Savage, and Lewis Alcott for useful comments. JBR would like to thank Huiming Bao for editorial handling and Laurence Coogan and three anonymous reviews for helpful comments. JBR was supported by a NERC GW4 + Doctoral Training Partnership studentship from the Natural Environmental Research Council [NE/S007504/1]. JBR, MBA, and TE acknowledge funding from a NERC grant [NE/T012595/1 & NE/T012633/1].

Appendix A. Supplementary Material

Supplementary Material related to this article can be found online at:

References

Algeo, T. J., and C. Li, 2020, Redox classification and calibration of redox thresholds in sedimentary systems: Geochimica et Cosmochimica Acta, **287**, 8–26.

Alt, J., 2004, Alteration of the upper oceanic crust: mineralogy, chemistry, and processes: Hydrogeology of the Oceanic Lithosphere, 456–488.

Alt, J. C., and J. Honnorez, 1984, Alteration of the upper oceanic crust, DSDP site 417: mineralogy and chemistry: Contributions to Mineralogy and Petrology, **87**, 149–169.

Alt, J. C., and D. A. H. Teagle, 2003, Hydrothermal alteration of upper oceanic crust formed at a fast-spreading ridge: mineral, chemical, and isotopic evidence from ODP Site 801: Chemical Geology, **201**, 191–211.

Alt, J. C., C. Laverne, R. M. Coggon, D. A. H. Teagle, N. R. Banerjee, S. Morgan, C. E. Smith-Duque, M. Harris, and L. Galli, 2010, Subsurface structure of a submarine hydrothermal system in ocean crust formed at the East Pacific Rise, ODP/IODP Site 1256: Submarine hydrothermal system: Geochemistry, Geophysics, Geosystems, **11**, Q10010.

Andersen, M. B., S. Romaniello, D. Vance, S. H. Little, R. Herdman, and T. W. Lyons, 2014, A modern framework for the interpretation of $^{238}U/^{235}U$ in studies of ancient ocean redox: Earth and Planetary Science Letters, **400**, 184–194.

Andersen, M. B., T. Elliott, H. Freymuth, K. W. W. Sims, Y. Niu, and K. A. Kelley, 2015, The terrestrial uranium isotope cycle: Nature, **517**, 356–359.

Andersen, M. B., J. B. Rodney, H. Freymuth, F. Vils, M. Harris, K. Cooper, D. A. H. Teagle, and T. Elliott, 2024, Time scales and mechanisms of uranium uptake in altered ocean crust; observations from the ~15 million year-old site 1256 in the eastern equatorial Pacific: Geochimica et Cosmochimica Acta, **382**, 142–159.

Anderson, R. F., M. Q. Fleisher, and A. P. LeHuray, 1989, Concentration, oxidation state, and particulate flux of uranium in the Black Sea: Geochimica et Cosmochimica Acta, **53**, 2215–2224.

Bach, W., B. Peucker-Ehrenbrink, S. R. Hart, and J. S. Blusztajn, 2003, Geochemistry of hydrothermally altered oceanic crust: DSDP/ODP Hole 504B - Implications for seawater-crust exchange budgets and Sr- and Pb-isotopic evolution of the mantle: Hydrothermally altered oceanic crust: Geochemistry, Geophysics, Geosystems, **4**, 8904.

869 Bacon, M. P., 1978, Radioactive disequilibrium in altered mid-oceanic basalts: Earth and
870 Planetary Science Letters, **39**, 250–254.
871 Butterfield, N. J., 2007, Macroevolution and Macroecology Through Deep Time:
872 Palaeontology, **50**, 41–55.
873 Canfield, D. E., 1998, A new model for Proterozoic ocean chemistry: Nature, **396**, 450–453.
874 Canfield, D. E., 2014, 6.8 - Proterozoic Atmospheric Oxygen, *in* H. D. Holland and K. K.
875 Turekian, eds., Treatise on Geochemistry (Second Edition), Elsevier, 197–216.
876 Canfield, D. E., S. W. Poulton, and G. M. Narbonne, 2007, Late-Neoproterozoic Deep-Ocean
877 Oxygenation and the Rise of Animal Life: Science, **315**, 92–95.
878 Canfield, D. E., S. W. Poulton, A. H. Knoll, G. M. Narbonne, G. Ross, T. Goldberg, and H.
879 Strauss, 2008, Ferruginous conditions dominated later neoproterozoic deep-water
880 chemistry: Science (New York, N.Y.), **321**, 949–952.
881 Chabaux, F., J. Riotte, and O. Dequincey, 2003, U-Th-Ra Fractionation During Weathering
882 and River Transport: Reviews in Mineralogy and Geochemistry, **52**, 533–576.
883 Chen, B., C. Hu, B. J. W. Mills, T. He, M. B. Andersen, X. Chen, P. Liu, M. Lu, R. J. Newton,
884 S. W. Poulton, G. A. Shields, and M. Zhu, 2022, A short-lived oxidation event during
885 the early Ediacaran and delayed oxygenation of the Proterozoic ocean: Earth and
886 Planetary Science Letters, **577**, 117274.
887 Cheng, H., R. Lawrence Edwards, C.-C. Shen, V. J. Polyak, Y. Asmerom, J. Woodhead, J.
888 Hellstrom, Y. Wang, X. Kong, C. Spötl, X. Wang, and E. Calvin Alexander, 2013,
889 Improvements in ^{230}Th dating, ^{230}Th and ^{234}U half-life values, and U–Th isotopic
890 measurements by multi-collector inductively coupled plasma mass spectrometry: Earth
891 and Planetary Science Letters, **371–372**, 82–91.
892 Dahl, T. W., R. A. Boyle, D. E. Canfield, J. N. Connelly, B. C. Gill, T. M. Lenton, and M.
893 Bizzarro, 2014, Uranium isotopes distinguish two geochemically distinct stages during
894 the later Cambrian SPICE event: Earth and Planetary Science Letters, **401**, 313–326.
895 Dahl, T. W., E. U. Hammarlund, A. D. Anbar, D. P. G. Bond, B. C. Gill, G. W. Gordon, A. H.
896 Knoll, A. T. Nielsen, N. H. Schovsbo, and D. E. Canfield, 2010, Devonian rise in
897 atmospheric oxygen correlated to the radiations of terrestrial plants and large predatory
898 fish: Proceedings of the National Academy of Sciences, **107**, 17911–17915.
899 Dang, D. H., W. Wang, T. M. Gibson, M. Kunzmann, M. B. Andersen, G. P. Halverson, and
900 R. D. Evans, 2022, Authigenic uranium isotopes of late Proterozoic black shale:
901 Chemical Geology, **588**, 120644.

902 Dunk, R. M., R. A. Mills, and W. J. Jenkins, 2002, A reevaluation of the oceanic uranium
903 budget for the Holocene: Chemical Geology, **190**, 45–67.
904 Dunning, G., and T. Krogh, 1985, Geochronology of ophiolites of the Newfoundland
905 Appalachians: Canadian Journal of Earth Sciences, **22**, 1659–1670.
906 Gale, A., C. A. Dalton, C. H. Langmuir, Y. Su, and J.-G. Schilling, 2013, The mean
907 composition of ocean ridge basalts: Geochemistry, Geophysics, Geosystems, **14**, 489–
908 518.
909 Gaschnig, R. M., C. T. Reinhard, N. J. Planavsky, X. Wang, D. Asael, and M. G. Jackson,
910 2021, The impact of primary processes and secondary alteration on the stable isotope
911 composition of ocean island basalts: Chemical Geology, **581**, 120416.
912 Gianola, O., M. W. Schmidt, O. Jagoutz, J. Rickli, O. Bruguier, and O. Sambuu, 2019, The
913 Crust–Mantle Transition of the Khantaishir Arc Ophiolite (Western Mongolia): Journal
914 of Petrology, **60**, 673–700.
915 Gillis, K. M., L. A. Coogan, and C. Brant, 2015, The role of sedimentation history and lithology
916 on fluid flow and reactions in off-axis hydrothermal systems: A perspective from the
917 Troodos ophiolite: Chemical Geology, **414**, 84–94.
918 Hart, S. R., and H. Staudigel, 1982, The control of alkalies and uranium in seawater by ocean
919 crust alteration: Earth and Planetary Science Letters, **58**, 202–212.
920 Holland, H. D., 1984, The Chemical Evolution of the Atmosphere and Oceans: Princeton Univ.
921 Press, Princeton.
922 Jian, P., A. Kröner, B. Jahn, B. Windley, Y. Shi, W. Zhang, F. Zhang, L. Miao, D. Tomurhuu,
923 and D. Liu, 2014, Zircon dating of Neoproterozoic and Cambrian ophiolites in West
924 Mongolia and implications for the timing of orogenic processes in the central part of
925 the Central Asian Orogenic Belt: Earth-Science Reviews, **133**.
926 Kelley, K. A., T. Plank, J. Ludden, and H. Staudigel, 2003, Composition of altered oceanic
927 crust at ODP Sites 801 and 1149: Geochemistry, Geophysics, Geosystems, **4**, 8910.
928 Kipp, M. A., H. Li, M. J. Ellwood, S. G. John, R. Middag, J. F. Adkins, and F. L. H. Tissot,
929 2022, 238U, 235U and 234U in seawater and deep-sea corals: A high-precision
930 reappraisal: Geochimica et Cosmochimica Acta, **336**, 231–248.
931 Klinkhammer, G. P., and M. R. Palmer, 1991, Uranium in the oceans: Where it goes and why:
932 Geochimica et Cosmochimica Acta, **55**, 1799–1806.
933 Krause, A. J., B. J. W. Mills, A. S. Merdith, T. M. Lenton, and S. W. Poulton, 2022, Extreme
934 variability in atmospheric oxygen levels in the late Precambrian: Science Advances, **8**,
935 eabm8191.

936 Krause, A. J., B. J. W. Mills, S. Zhang, N. J. Planavsky, T. M. Lenton, and S. W. Poulton,
937 2018, Stepwise oxygenation of the Paleozoic atmosphere: Nature Communications, **9**,
938 4081.
939 Kröner, A., W. Todt, I. M. Hussein, M. Mansour, and A. A. Rashwan, 1992, Dating of late
940 Proterozoic ophiolites in Egypt and the Sudan using the single grain zircon evaporation
941 technique: Precambrian Research, **59**, 15–32.
942 Langmuir, D., 1978, Uranium solution-mineral equilibria at low temperatures with applications
943 to sedimentary ore deposits: Geochimica et Cosmochimica Acta, **42**, 547–569.
944 Lenton, T. M., R. A. Boyle, S. W. Poulton, G. A. Shields-Zhou, and N. J. Butterfield, 2014,
945 Co-evolution of eukaryotes and ocean oxygenation in the Neoproterozoic era: Nature
946 Geoscience, **7**, 257–265.
947 Lissenberg, C. J., J. H. Bédard, and C. R. van Staal, 2004, The structure and geochemistry of
948 the gabbro zone of the Annieopsquotch ophiolite, Newfoundland: implications for
949 lower crustal accretion at spreading ridges: Earth and Planetary Science Letters, **229**,
950 105–123.
951 Lissenberg, C. J., C. R. van Staal, J. H. Bédard, and A. Zagorevski, 2005, Geochemical
952 constraints on the origin of the Annieopsquotch ophiolite belt, Newfoundland
953 Appalachians: Geological Society of America Bulletin, **117**, 1413.
954 Lyons, T. W., C. T. Reinhard, and N. J. Planavsky, 2014, The rise of oxygen in Earth's early
955 ocean and atmosphere: Nature, **506**, 307–315.
956 Lyons, T. W., C. W. Diamond, N. J. Planavsky, C. T. Reinhard, and C. Li, 2021, Oxygenation,
957 Life, and the Planetary System during Earth's Middle History: An Overview:
958 Astrobiology, **21**, 906–923.
959 Lyons, T. W., C. J. Tino, G. P. Fournier, R. E. Anderson, W. D. Leavitt, K. O. Konhauser, and
960 E. E. Stüeken, 2024, Co-evolution of early Earth environments and microbial life:
961 Nature Reviews Microbiology, **22**, 572–586.
962 MacDougall, J. D., R. C. Finkel, J. Carlson, and S. Krishnaswami, 1979, Isotopic evidence for
963 uranium exchange during low-temperature alteration of oceanic basalt: Earth and
964 Planetary Science Letters, **42**, 27–34.
965 Mills, B. J. W., A. J. Krause, I. Jarvis, and B. D. Cramer, 2023, Evolution of Atmospheric O2
966 Through the Phanerozoic, Revisited: Annual Review of Earth and Planetary Sciences,
967 **51**, 253–276.
968 Noordmann, J., S. Weyer, R. B. Georg, S. Jöns, and M. Sharma, 2016, $^{(238)}U/^{(235)}U$ isotope
969 ratios of crustal material, rivers and products of hydrothermal alteration: new insights

970 on the oceanic U isotope mass balance: Isotopes in Environmental and Health Studies,
971 **52**, 141–163.
972 Osmond, J. K., and J. B. Cowart, 1976, The theory and uses of natural uranium isotopic
973 variations in hydrology: Atomic Energy Review, **14**, 621–679.
974 Partin, C. A., A. Bekker, N. J. Planavsky, C. T. Scott, B. C. Gill, C. Li, V. Podkovyrov, A.
975 Maslov, K. O. Konhauser, S. V. Lalonde, G. D. Love, S. W. Poulton, and T. W. Lyons,
976 2013, Large-scale fluctuations in Precambrian atmospheric and oceanic oxygen levels
977 from the record of U in shales: Earth and Planetary Science Letters, **369–370**, 284–293.
978 Pavia, F. J., E. H. G. Cooperdock, J. C. de Obeso, K. W. W. Sims, F. L. H. Tissot, and F. Klein,
979 2023, Uranium isotopes as tracers of serpentinite weathering: Earth and Planetary
980 Science Letters, **623**, 118434.
981 Planavsky, N. J., C. T. Reinhard, X. Wang, D. Thomson, P. McGoldrick, R. H. Rainbird, T.
982 Johnson, W. W. Fischer, and T. W. Lyons, 2014, Low Mid-Proterozoic atmospheric
983 oxygen levels and the delayed rise of animals: Science, **346**, 635–638.
984 Planavsky, N. J., P. McGoldrick, C. T. Scott, C. Li, C. T. Reinhard, A. E. Kelly, X. Chu, A.
985 Bekker, G. D. Love, and T. W. Lyons, 2011, Widespread iron-rich conditions in the
986 mid-Proterozoic ocean: Nature, **477**, 448–451.
987 Regelous, M., K. M. Haase, S. Freund, M. Keith, C. G. Weinzierl, C. Beier, P. A. Brandl, T.
988 Endres, and H. Schmidt, 2014, Formation of the Troodos Ophiolite at a triple junction:
989 Evidence from trace elements in volcanic glass: Chemical Geology, **386**, 66–79.
990 Richter, S., A. Alonso-Munoz, R. Eykens, U. Jacobsson, H. Kuehn, A. Verbruggen, Y. Aregbe,
991 R. Wellum, and E. Keegan, 2008, The isotopic composition of natural uranium samples
992 - Measurements using the new $n^{(233U)}/n^{(236U)}$ double spike IRMM-3636: International
993 Journal of Mass Spectrometry, **269**, 145–148.
994 Robbins, L. J., S. V. Lalonde, N. J. Planavsky, C. A. Partin, C. T. Reinhard, B. Kendall, C.
995 Scott, D. S. Hardisty, B. C. Gill, D. S. Alessi, C. L. Dupont, M. A. Saito, S. A. Crowe,
996 S. W. Poulton, A. Bekker, T. W. Lyons, and K. O. Konhauser, 2016, Trace elements at
997 the intersection of marine biological and geochemical evolution: Earth-Science
998 Reviews, **163**, 323–348.
999 Sahoo, S. K., N. J. Planavsky, G. Jiang, B. Kendall, J. D. Owens, X. Wang, X. Shi, A. D.
1000 Anbar, and T. W. Lyons, 2016, Oceanic oxygenation events in the anoxic Ediacaran
1001 ocean: Geobiology, **14**, 457–468.
1002 Scott, C., T. W. Lyons, A. Bekker, Y. Shen, S. W. Poulton, X. Chu, and A. D. Anbar, 2008,
1003 Tracing the stepwise oxygenation of the Proterozoic ocean: Nature, **452**, 456–459.

Seyedali, M., L. A. Coogan, and K. M. Gillis, 2021, Li-isotope exchange during low-temperature alteration of the upper oceanic crust at DSDP Sites 417 and 418: Geochimica et Cosmochimica Acta, **294**, 160–173.

Sperling, E. A., C. J. Wolock, A. S. Morgan, B. C. Gill, M. Kunzmann, G. P. Halverson, F. A. Macdonald, A. H. Knoll, and D. T. Johnston, 2015, Statistical analysis of iron geochemical data suggests limited late Proterozoic oxygenation: Nature, **523**, 451–454.

Stockey, R. G., D. B. Cole, U. C. Farrell, H. Agić, T. H. Boag, J. J. Brocks, D. E. Canfield, M. Cheng, P. W. Crockford, H. Cui, T. W. Dahl, L. Del Mouro, K. Dewing, S. Q. Dornbos, J. F. Emmings, R. R. Gaines, T. M. Gibson, B. C. Gill, G. J. Gilleaudeau, K. Goldberg, R. Guilbaud, G. Halverson, E. U. Hammarlund, K. Hantsoo, M. A. Henderson, C. M. Henderson, M. S. W. Hodgskiss, A. J. M. Jarrett, D. T. Johnston, P. Kabanov, J. Kimmig, A. H. Knoll, M. Kunzmann, M. A. LeRoy, C. Li, D. K. Loydell, F. A. Macdonald, J. M. Magnall, N. T. Mills, L. M. Och, B. O'Connell, A. Pagès, S. E. Peters, S. M. Porter, S. W. Poulton, S. R. Ritzer, A. D. Rooney, S. Schoepfer, E. F. Smith, J. V. Strauss, G. J. Uhlein, T. White, R. A. Wood, C. R. Woltz, I. Yurchenko, N. J. Planavsky, and E. A. Sperling, 2024, Sustained increases in atmospheric oxygen and marine productivity in the Neoproterozoic and Palaeozoic eras: Nature Geoscience, **17**, 667–674.

Stolper, D. A., and C. B. Keller, 2018, A record of deep-ocean dissolved O_2 from the oxidation state of iron in submarine basalts: Nature, **553**, 323–327.

Stolper, D. A., X. Pu, M. K. Lloyd, N. I. Christensen, C. E. Bucholz, and R. A. Lange, 2022, Constraints on Early Paleozoic Deep-Ocean Oxygen Concentrations From the Iron Geochemistry of the Bay of Islands Ophiolite: Geochemistry, Geophysics, Geosystems, **23**, e2021GC010196.

Sylwester, E. R., E. A. Hudson, and P. G. Allen, 2000, The structure of uranium (VI) sorption complexes on silica, alumina, and montmorillonite: Geochimica et Cosmochimica Acta, **64**, 2431–2438.

Thurber, D. L., 1962, Anomalous U 234 U 238 in nature: Journal of Geophysical Research, **67**, 11, 4518-4520.

Tostevin, R., and B. J. W. Mills, 2020, Reconciling proxy records and models of Earth's oxygenation during the Neoproterozoic and Palaeozoic: Interface Focus, **10**, 20190137.

Wei, G.-Y., N. J. Planavsky, T. He, F. Zhang, R. G. Stockey, D. B. Cole, Y.-B. Lin, and H.-F. Ling, 2021, Global marine redox evolution from the late Neoproterozoic to the early

Paleozoic constrained by the integration of Mo and U isotope records: Earth-Science Reviews, **214**, 103506.

Zimmer, M., A. Kröner, K. P. Jochum, T. Reischmann, and W. Todt, 1995, The Gabal Gerf complex: A precambrian N-MORB ophiolite in the Nubian Shield, NE Africa: Chemical Geology, **123**, 29–51.